HHS Public Access

Author manuscript

Int J Min Sci Technol. Author manuscript; available in PMC 2016 April 20.

Published in final edited form as:

Int J Min Sci Technol. 2016 January ; 26(1): 123–130. doi:10.1016/j.ijmst.2015.11.020.

Volumetric measurement of rock movement using photogrammetry

Donovan J. Benton[*], **Stephen R. Iverson**, **Lewis A. Martin**, **Jeffrey C. Johnson**, and **Michael J. Raffaldi**

National Institute for Occupational Safety and Health, Spokane 99207, USA

Abstract

NIOSH ground control safety research program at Spokane, Washington, is exploring applications of photogrammetry to rock mass and support monitoring. This paper describes two ways photogrammetric techniques are being used. First, photogrammetric data of laboratory testing is being used to correlate energy input and support deformation. This information can be used to infer remaining support toughness after ground deformation events. This technique is also demonstrated in a field application. Second, field photogrammetric data is compared to crackmeter data from a deep underground mine. Accuracies were found to average 8 mm, but have produced results within 0.2 mm of true displacement, as measured by crackmeters. Application of these techniques consists of monitoring overall fault activity by monitoring multiple points around the crackmeter. A case study is provided in which a crackmeter is clearly shown to have provided insufficient information regarding overall fault ground deformation. Photogrammetry is proving to be a useful ground monitoring tool due to its unobtrusiveness and ease of use.

Keywords

Photogrammetry; Ground control; Monitoring; Deep vein mining; Volume calculation; Crackmeter

1. Introduction

1.1. NIOSH mine safety research

Photogrammetry systems have been implemented by the National Institute for Occupational Safety and Health (NIOSH) as part of its ground control research to improve mine safety. Conventional monitoring of ground movement has typically focused on movement of a few discrete points that are marked or anchored to instruments. Loss of a designated point or anchor, or the ability to identify a stable point in an unstable area, has often frustrated monitoring efforts. NIOSH researchers are using photogrammetry to conduct full-field measurements of rock surfaces underground. Periodic measurements of the entire surface of a ramp allow patterns of displacement to be observed. Full-field measurements provide much more insight into ground behavior than point measurements.

[*]Corresponding author. Tel.: +1 5093548085. xfu5@cdc.gov. .

1.2. Background

Previous work by Benton, et al. discussed laboratory calibration and verification testing of two photogrammetry systems being used by NIOSH researchers [1]. Both systems utilize stereoscopic image pairing techniques for photogrammetric reconstruction. This paper discusses how a laboratory system was used to conduct volumetric analyses of testing of shotcrete panels with varying types of reinforcement. The laboratory system was found to be accurate to within 2 mm. Additionally, a field photogrammetry system was found to produce linear measurements within 1 mm of known lengths in laboratory conditions. This system is currently being used at a deep underground mine to observe ground support conditions and deformations that have occurred. This paper discusses comparison of preliminary volumetric measurements of rib deformation to laboratory tests, as well as comparison of the field system against a crackmeter installed across a fault surface where it intersects the ramp.

2. Photogrammetric volume calculations

2.1. High energy, high deformation testing

Ground control safety often depends on supporting, or at least containing, the ground between rock bolts. Shotcrete and mesh, in various combinations and with other components, are often called upon to do this, as shown in Fig. 1.

Applications are especially common in mines with squeezing ground or seismic loading. The combination of mesh and shotcrete forms a panel, or plate, that is typically bent by ground extruding between restraining rock bolts. The resistance of these panels to bending across large ground deformations is important for maintaining ground support safety. Combinations of shotcrete, mesh and other components that can maintain significant support pressure are desired, a characteristic described as the “toughness” of support. Toughness can be quantified as the work done during deformation (e.g., force x displacement). However, the toughness of a design is difficult to estimate. NIOSH researchers have responded to this deficiency by designing a full-scale test device.

Previous testing of total system toughness has been completed by Kirsten and Tannant and Kaiser [3–5]. However, the test “stroke” or maximum displacement fell far short of displacement magnitudes observed in-situ. As such, a test device was needed to measure high resistance energies (toughness) over high displacements. A combination dubbed high-energy high-displacement (HEHD) incorporated these alterations [6]. First, a stroke of 25 cm was specified, roughly doubling the test stroke of previous systems. Second, the scale of testing was expanded somewhat to accommodate a 1.2 m bolt pattern while minimizing edge effects. Finally, better information on deformation volume changes and crack geometry was desired for comparison with test observations.

2.2. Photogrammetry application to shotcrete panel testing

Photogrammetric observation of HEHD panel testing was conducted to track deformation volume changes. This information could then be used to delineate the relationship between reinforced shotcrete “bulge” deformation between rock bolts and residual toughness of the intact support. This can be done by correlating volumetric displacements of shotcrete panels

with known displacements and loads obtained during panel tests. This technique may also be applied to mesh or reinforced shotcrete installed in a mine to infer remaining support toughness from observed volumetric changes. This is particularly important knowledge where seismic loading may impart significant energy to the support system; thus, photogrammetric methods can aid in designing a safe work site.

A laboratory photogrammetry system developed by NIOSH researchers allows for documentation of tests [1]. This system has been used during HEHD shotcrete panel tests. The laboratory photogrammetric system consists of two Nikon® D800 digital SLR cameras, each mounted with a Sigma 20 mm prime wide angle lens. 3DM CalibCam camera calibration software and 3DM analyst photogrammetry software from Adam Technology® were used to complete the 3D reconstructions of laboratory testing [7]. Each test included capturing left and right images at one-second intervals. Camera clock times were synchronized with the data acquisition system clock times immediately prior to each test.

The HEHD testing process begins as aspherically-shaped hydraulic ram head is pushed through the test panel while being restrained by paddle anchor D-Bolts® embedded in the four columns of the test frame, as shown in Fig. 2.

D-Bolts are designed specifically to absorb energy in dynamically loaded rock masses [8]. Load and displacement data are collected during the test using an advanced data acquisition system. Once the ram reached 25 cm displacement, the system was de-energized and photogrammetric monitoring ended.

2.3. Photogrammetry data analysis

Photographic image pairs were selected at 5 cm ram displacement intervals. These pairs were reconstructed in 3D for volumetric analysis. The top corners of the shotcrete panels were used as control points for scale and orientation. Camera calibrations, images and control points were input into the software. The reconstruction process was conducted in four steps for each test:

- **(a)** Locate the control points on the first image pair.
- **(b)** Find relative points between image pairs.
- **(c)** Run the bundle adjustment with control points for the first image pair with known camera locations for subsequent image pairs.
- **(d)** Construct the digital terrain models for each interval.

The models were then trimmed to remove extraneous points prior to comparing volumes. The Adam Technology software has a built-in volume calculation function that determines maximum height and volume calculations from a defined base plane, which in this case was set to the plane defined by the four control points and the zero elevation.

2.4. Volume-energy relationship analysis

Volume-energy relationship analyses were conducted for three types of shotcrete panels. A weakest-to-strongest spectrum for analysis was created by using a panel made of a standard

shotcrete mix (no reinforcement), one made of poly-fiber shotcrete mix (fiber reinforced), and a third made with cyclone fencing enclosed in a fiber shotcrete mix (mesh and fiber reinforced). An additional test using only a 1.8 m × 1.8 m cyclone fence piece with no shotcrete was conducted as a baseline. This test used a piece of burlap underneath the fencing to provide an adequate background for photogrammetric reconstruction. The burlap's influence on fence performance was judged to be negligible. The cyclone fence test also used a 1.2 m bolt spacing to replicate mine application. Synchronized clock times were established prior to each test between the cameras and data logger. The load and displacement data for each test were used to calculate energy, which was then matched with digitally recorded time stamps for each photograph pair. These data were used to match photogrammetric data with the calculated energy data at 5 cm ram displacement intervals. Corresponding deformation volumes acquired through photogrammetric measurement were then compared to energy calculations for each interval.

Finally, measurement errors were assessed. Panel and fence surface roughness, precise manual selection of control points, and software determination of zero on the vertical axis from these control points all result in small volume discrepancies. The average measurement error of this system has been shown to be 2 mm, resulting in a percentage error of ± 1.8%. These factors were accounted for by zeroing volume and height measurements around the assumed base level measurements, and then adjusting each result. The raw data from the shotcrete panel analyses can be seen in Table 1, and the data from the mesh tests can be shown in Table 2. Minimum and maximum volumes, as well as energy are shown for each displacement interval.

By observing the data in Table 1, one can see that panel volumes remained relatively constant for each interval, regardless of panel type. This was expected because both dimensional measurements were based on similar ram displacements. The slight variability in volume and height are due to panel surface texture and geometry of panel failure. Deformation profiles of each panel type at 25 cm ram displacement are shown in Fig. 3.

The standard mix shotcrete panel (1) underwent more widespread deformation than either the fiber mix (2) or cyclone in fiber mix (3) panels. The standard mix panel experienced deformation along its entire profile, while the cyclone reinforced fiber mix panel remained relatively stationary at their edges. This observation is reflected in the volume calculations for each panel at final deformation, where the standard mix panel has the highest result. Deformation profiles of the two mesh types are not included, as they merely assumed the contours of the ram head.

More significant, however, is the relationship between deformation volume, deformation height, and energy. Fig. 4 shows volume-energy relationship. The effect of shotcrete reinforcement is clear in terms of energy absorption capacity.

Cyclone-reinforced fiber shotcrete can withstand energies over 400% greater than standard mix shotcrete while undergoing the same volume of deformation. A clear difference in performance between the three types of shotcrete can be identified from this analysis. Assuming a 1.2 m × 1.2 m bolt spacing pattern, the potential exists for a yield "volume" to

be assessed in field settings. While standard and fiber mix shotcretes appear to lose load-bearing capacity at deformation volumes of 0.10 m^3, cyclone-reinforced fiber shotcrete can still assume more loading even at deformation volumes of 0.25 m^3. At present, it is not possible to determine whether the better performance of cyclone-reinforced fiber shotcrete is the result of fencing reinforcement, or the fiber in combination with the fencing. Future tests of cyclone-reinforced standard mix shotcrete panels still need to be conducted.

The cyclone fence test provided less conclusive results. It required approximately 9 cm of ram displacement before the fencing started to provide significant resistance. This is due to the fact that the fencing is relatively loose and that there is play in the system until the links make contact/interlock and start to develop tension in the steel strands. The force then begins to increase linearly with further displacement as the chain link fence begins to tighten and the wire strands are loaded in tension within their elastic region. With enough displacement, the chain link fence would be expected to exhibit ductile deformation. The welded wire mesh tests provided slightly better results, requiring less displacement (3 cm) before reaction began. However, no point of failure was reached, due to the same factors that limited the cyclone fence testing. Without shotcrete, both types of mesh have, on their own, essentially no load carrying capacity until excessive deformations occur. Since the test stopped at 25 cm of displacement, behavior of the cyclone fencing and welded wire mesh at failure was not observed. The energy-volume relationship for each type of mesh can be seen in Fig. 5.

2.5. Field volume measurements

Field deformation volumes were calculated similarly to laboratory testing volumes. Site selection was based on two factors: range of deformation at the site, and orientation of bedding planes. The chosen site displayed varying levels of deformation ranging from minor (<3 cm) to severe (>30 cm). Areas of the rib with roughly 1.8 by 1.8 m sides were chosen for both minor and severe cases of deformation, as well as an additional area of significant (approximately 15 cm) deformation. These areas are shown in Fig. 6, with Area 1 representing significant deformation, and Areas 2 and 3 representing severe and minor deformation, respectively.

As noted in Fig. 6, Areas 1, 2 and 3 correspond to significant (approximately 15 cm), severe (approximately 30 cm), and minor (approximately 3 cm) deformation, respectively.

Additionally, bedding planes at the site were parallel to the rib face, an orientation that leads to greater deformation. Parallel bedding also allowed for the closest comparison to be made of field deformations to laboratory panel testing.

Following techniques used in laboratory volume measurements, each 1.8 m × 1.8 m area of the field site was considered as a uniform “panel” securely pinned by bolts at its corners. The volume of “bagged” or “bulged” material within the perimeter of bolts was treated as the bulge deformation of the shotcrete panels. It should be made clear, however, that cyclone fencing only, and not shotcrete, was used for surface control at this particular field site. Agisoft® Photo Scan Professional Edition was used for field volume calculations. This software is more amenable to field calculations because before-and-after reconstructions are not needed to calculate volumes. Surfaces of bulging material can be isolated, trimmed and

transformed into standalone solids by bridging low points along the perimeter across the area. Side views of each area are shown in Fig. 7.

As shown in Fig. 7, Areas 1, 2 and 3 correspond to slabbing, fractured and competent rock masses, respectively.

Area 1 was composed of loose slabs being pushed out between bolts, while Area 2 was primarily highly fractured material bagging in the mesh between the bolts. Conversely, Area 3 consisted of competent rock, with minimal extrusion between bolts. The volume calculations and related estimations of energy for each area can be seen in Table 3.

Energy estimations were calculated by interpolating the data obtained from laboratory testing of cyclone mesh, shown previously in Fig. 4. Due to unreliability of data for displacements less than 15 cm, the energy for Area 3 could only be estimated as less than 100 J. Confidence in the accuracy of the calculated volumes is based on their apparent correlation with volumes calculations derived from laboratory testing of panels having similar 1.8 by 1.8 m surface areas. Refinement of field volume calculations would include calibration and optimization of Agisoft's Photo Scan software in both laboratory and field settings. Further applications of these techniques include usage at shotcrete reinforced sites, and calculations of volume loss in areas of key blocking. At present, photogrammetric calculations of deformation volumes appear as a viable technique for understanding rock mass behavior and increasing information for use in ground control safety.

3. Photogrammetric monitoring of fault movement

3.1. Field photogrammetry system

A Nikon® D80 digital SLR camera with a Sigma 10 to 20 mm zoom lens was used for the majority of the field surveys discussed in this paper. A Canon® EOS 5D Mark III camera has been used for field surveys since January 2015, which provides higher quality data for photogrammetric reconstruction of scenes. A comparison of the cameras can be seen in Table 4.

Shape Metrix^{3D} photogrammetry software from 3GSM was used to complete the 3D field site reconstructions. The software was developed specifically for mining and construction applications and includes a camera/lens calibration. The system hardware includes a camera, lens, tripod and a survey range pole. Auxiliary lighting for measurement sites was provided by three Pelican® 9430 Remote Area Lighting Systems (RALS). The RALS generated enough lighting to capture the true color and fine detail of the rock surfaces and support systems; they remained stationary during each photogrammetric session and had sufficient battery power for day-length surveys. Camera settings were selected to provide the best image quality, including low ISO (generally 100) and medium f-stop (typically 8). The expected slow camera shutter speeds at these settings required a tripod to prevent movement during image capture.

3.2. Fault monitoring

Site measurements made using the field photogrammetry system were compared to crackmeter data from the deep underground mine. The participating mine uses Geokon® model 4420 vibrating wire crackmeters to monitor fault movement. These meters are designed specifically for monitoring movement across natural rock joints in the civil and mining industries. As shown in Fig. 8, each crackmeter consists of a vibrating wire displacement transducer contained within a stainless steel housing rod.

The displacement transducer is a vibrating wire sensing element with a spring connected to one end and a rod connected to the other. The instrument is placed across the joint of interest and anchored into the rock.

As movement occurs along the joint, the connecting rod is displaced from the body of the gauge causing an increase or decrease in tension in the wire. This change in tension is directly proportional to the extension or compression, allowing the movement along the fault to be determined. The frequency measurements are converted to displacements via manufacturer-calibrated gage factors and the difference between the current and initial reading at the time of installation.

The crackmeters are accurate to within ± 0.1% of the full scale or total range of the instrument. The participating mine uses crackmeters of 100 and 150 cm lengths. Thus, the mine instrumentation has an accuracy of 1.0–1.5 mm, roughly the same accuracy as the NIOSH field photogrammetry system.

3.3. Crackmeter monitoring

Quarterly photogrammetric surveys of three separate fault structures at the participating mine have been conducted, beginning in January 2013. The mine in this study has three faults intercepted by a ramp system at nine locations, spanning seven levels, with no more than one fault structure at each site. Most of these sites have crackmeters installed across the exposed fault. Initially seven crackmeters were installed at the survey sites. All seven crackmeters were operational through October 2014. At this time, one of the crackmeters stopped producing data as a result of damage to the communications wire.

A photogrammetric reconstruction was completed for each individual crackmeter, creating a “virtual” crackmeter for analysis within a 3D point cloud. Mine survey data are then used to reference each photogrammetry survey to global coordinates, thus scaling each virtual crackmeter. Photogrammetric measurements of the crackmeters are made within the Shape Metrix^{3D} software by affixing a measuring point to each end. The scene depicted in Fig. 9 is a reconstruction of a crackmeter location.

As noted in Fig. 9, length measurements are made using points (red dots).

The red dots represent the Shape Metrix^{3D} measuring points, and the yellow dashed line marks the distance between the measuring points. The coordinates of the measuring points give the location of the crackmeter anchors in 3D space, and can be used to determine length, location, and orientation.

Virtual crackmeter data can be compared to real instrument data. Over time, changes in length, location, and orientation constitute displacement of the rock masses on either side of the fault. Crackmeter data is obtained from the mine and compared to photogrammetric measurements. A total of 70 measurement comparisons have been completed between October 2013 and January 2015. The point array in Fig. 10 represents the absolute error of the photogrammetric measurements versus the actual displacement as determined by the crackmeters. The average photogrammetric error, corrected to two standard deviations (24.8 mm), is roughly 8.0 mm, five to eight times that of the crackmeter error (1.0–1.5 mm).

Several variables have been investigated as causes of this additional error. Fig. 10 codes absolute error in terms of depth-to-base (D:B) ratio, which is the distance to the target relative to the spacing between cameras. The red markers indicate measurements made using D:B ratios between 6.0 and 9.9, typically the optimal range. Differing demands of area coverage and site accessibility made it difficult to stay in this range, thus there were a significant number of measurements made using D:B ratios less than 6.0, or greater than 9.9. Curiously however, as can be seen in Fig. 5, D:B ratios between 6.0 and 9.9 actually produced less accurate measurements (average 9.32 mm error) than D:B ratios outside the range (average 6.24 mm error). The crackmeter's shape and appearance is the probable cause for this discrepancy.

Higher D:B ratios tend to provide more planimetric (perpendicular field) accuracy, while lower ratios provide more depth (parallel field) accuracy. Ratios between 6.0 and 10.0 generally provide the best compromise between these two types of accuracy. However, when an object occupies very little space in one or the other field, balancing the two may become less significant due to the loss of three-dimensionality of the object. As a result of the crackmeter's slenderness, it will appear more two-dimensional, thus reducing the importance of balancing planimetric and depth fields. Though a conclusion cannot presently be made, it may even be the case that favoring one field over the other, depending on crackmeter orientation would produce the best results, as indicated by Fig. 10.

Additionally, while fractured rock surfaces are ideal for photogrammetry due to non-uniformity of texture and color, the crackmeters are poor objects for photogrammetric reconstruction. Their smooth, slender, single-colored appearance introduces error in point identification during reconstruction and analysis. The projection of the crackmeters from the rock face introduces the issue of shadowing, wherein cameras cannot detect what is behind an object. The object itself is projected as a shadow, either displacing the object from its true position, or assimilating it with the background scene. There is also small amount of error (approximately 0.3 mm) associated with picking the end points of the crackmeter. These problems may be mitigated by the close-up technique mentioned earlier, but cannot be technologically eliminated at present. Affixing targets to the crackmeter ends during surveying may also be an option, but only if it can be done in a way that does not affect crackmeter performance.

3.4. A case study-5600 sublevel

Since crackmeters measure displacement in a single direction, the measurement is likely only a component of actual fault offset. Point cloud measurements provide a more complete

picture of 3D movements, e.g., folding and squeezing deformation. Photogrammetry's ability to observe changes in crackmeter location and orientation over time can provide additional information about rock mass movement. As mentioned previously, testing of photogrammetric measurements against crackmeter measurements revealed an average photogrammetric error of 8 mm. However, in cases where the "virtual" photogrammetric crackmeter nearly matched the behavior of the real crackmeter, additional site analyses may be performed with higher confidence. These analyses give truer information about the behavior of faults.

Conditions at the 5600 sublevel provided a good environment to test the capabilities of photogrammetric monitoring. Mine personnel observed severe stress-induced pillar deterioration that ultimately necessitated bypassing and backfilling the site [10]. Photogrammetric analysis was conducted to determine whether fault movement also influenced pillar deterioration.

Analysis of crackmeter data focuses on shortening and lengthening of the crackmeter. Depending on the orientation of the fault crossing the crackmeter, a sense of direction of fault motion can be ascertained. This technique is illustrated in Fig. 11.

In Scenario A, the initial crackmeter location (gold bar, October 2013) is oriented such that upward movement of the hanging wall would result in shortening of the crackmeter. The final crackmeter position (green bar, September 2014) represents the scene after movement has occurred. Alternatively, as shown in Scenario B, the footwall could have moved downwards, also resulting in a shortening of the crackmeter. In either scenario, the relative motion is the same, suggesting dip–slip offset of the fault.

However, analysis of the crackmeter data at the 5600 sublevel cannot account for other observed deformation. The approximately 30 cm of rib dilation observed by mine personnel indicates more significant movement than that registered by the crackmeter. In addition, photogrammetric survey data also indicated widespread movement, including rib dilation. To investigate this, global coordinates of each crackmeter anchor were used for a photogrammetric time lapse comparison between October 27, 2013 and September 28, 2014. During this period, the entire crackmeter was observed photogrammetrically to have moved an average of 24 cm outwards, and roughly 15.5 cm upwards.

Additional points on either side of the fault were selected for similar treatment. Global displacements for all these points were produced in mine global coordinates of easting, northing, and elevation (x, y, and z, respectively). To more fully understand fault activity at the 5600 sublevel site, the global x, y, and z displacements were transformed into local coordinate displacements oriented on strike and dip of the fault. Photogrammetric data indicated a strike of N63°E, which served as the new y-axis. A fault dip of 58° was used for the second transformation, which served as the direction of the new x-axis. The final x'', y'', and z'' axes represent movement in the dip, strike, and dilation orientations of the fault. All measurement points, both axis systems, and the left and right fault blocks are identified in Fig. 12.

As noted in Fig. 12, the thrust, slip, and convergence vectors of the fault are represented by x'', y'', and z'', respectively.

The axis transformations were calculated as follows:

$$\underline{u}'' = \underline{\underline{T}}\underline{u} \tag{1}$$

$$\underline{u}'' = \begin{bmatrix} u_{x''} \\ u_{y''} \\ u_{z''} \end{bmatrix} \tag{2}$$

$$\underline{u} = \begin{bmatrix} u_x \\ u_y \\ u_z \end{bmatrix} \tag{3}$$

$$\underline{\underline{T}} = \begin{bmatrix} cos\left(\vartheta_{y'}\right) & 0 & sin\left(\vartheta_{y'}\right) \\ 0 & 1 & 0 \\ -sin\left(\vartheta_{y'}\right) & 0 & cos\left(\vartheta_{y'}\right) \end{bmatrix} \begin{bmatrix} cos\left(\varphi_z\right) & sin\left(\varphi_z\right) & 0 \\ -sin\left(\varphi_z\right) & cos\left(\varphi_z\right) & 0 \\ 0 & 0 & 1 \end{bmatrix} \tag{4}$$

where $\underline{u}''$ is the displacements in the local coordinate system; $\underline{u}$ the displacements in the global coordinate system; $\underline{\underline{T}}$ the transformation matrix; ϕ_z the strike direction (rotation about the global Z-axis); and $\vartheta_{y'}$ the dip direction (rotation about the local y'-axis)

Another potential use for photogrammetric methods can be seen by this analysis. In Table 5, photogrammetric measurements of global displacements are compared to local displacements at the 5600 sublevel site.

As shown in Table 5, these displacements have been transformed into local coordinates to understand rock mass movement in the area.

Though crackmeter measurements indicated significant movement near the fault, they provided little information in terms of overall movement. Photogrammetric data indicated movement of both fault blocks in both the dip–slip ($+x''$) and the strike-slip vectors ($+y''$). The latter of these two photogrammetric observations seems to confirm mine personnel observations of rib convergence. Additionally, there appeared to be a slight separation of the right block from the left block in the dilation orientation (z''). This also confirms observations of skin deterioration, and the consequent apparent widening of the fault exposure. Overall, the primary rock mass movement appears to be rib convergence, with the apparent fault movement more likely being a result of movement in the skin of the excavation, rather than global fault offset.

Crackmeters can provide highly accurate local measurements in real time. Multitudes of crackmeters may also be used together to gain a sense of global movement trends. Photogrammetry cannot presently provide immediate data, and can suffer from significant interpretation times. Once photogrammetric data is interpreted, however, full-field deformations can be quantified. As seen in the 5600 sublevel case study, crackmeter data provided limited understanding of overall movement. While the crackmeter at this site did register significant movement, it missed rib deformation throughout the site. Photogrammetric data, on the other hand, measured this large-scale deformation. However, photogrammetric analysis was time-consuming, delaying insight into ground movement. It also could not discern how movement occurred over time, as photogrammetric data points correspond to discrete points in time. The full benefits of photogrammetry may thus be most apparent in volumetric monitoring as opposed to point-movement monitoring.

4. Conclusions

NIOSH researchers have successfully implemented a laboratory photogrammetry system in shotcrete panel and mesh support system testing to delineate the relationship between bulge deformation and remaining strength. Results showed that significant differences in toughness after deformation can be ascertained volumetrically for varying types of support. The results also indicated that yield volumes can be assessed in field settings. Field volume calculations showed the same potential to estimate energy release based on amount of bulge deformation between bolts. These photogrammetric techniques have potential to greatly increase the ability to assess field support conditions and requirements, and thus improve safety.

A separate photogrammetry system was found to reproduce field crackmeter readings to within 8.0 mm of known measurements. Variables significantly affecting accuracy, such as D:B ratios and object identification, have also been identified, with consideration given to how their effects may be minimized. Fault monitoring at the same mine has been conducted using photogrammetry, the results of which have been used to supplement crackmeter data. In two case studies, photogrammetry was found to confirm mine personnel observations of conditions, as well as supplement crackmeter interpretation. At one site, severe rib deformation was found to override crackmeter readings of fault movement. At a second site, fault movement indicated by crackmeter elongation was supported by photogrammetric observation. In both cases, photogrammetry showed significant potential to supplement crackmeter monitoring techniques.

NIOSH research of field and laboratory photogrammetric methods indicates the potential for photogrammetry to enhance ground deformation monitoring in underground mining. Utilization of this technology by the mining industry will improve analysis and response to changing ground conditions and, in turn, increase worker safety.

Acknowledgments

The authors gratefully acknowledge 3GSM and Adam Tech for their guidance and cooperation in this research. Cooperating industry entities who allowed access and assistance in field research are also gratefully acknowledged. The work described in this paper would not have been possible without their time and expertise. The authors also

acknowledge those who participated in the development of the HEHD testing system and construction of the shotcrete panels. Special thanks to the following NIOSH personnel: Curtis Clark, Michael Stepan, Marc Loken and Tex Kubacki for their laboratory assistance, Heather Lawson for her help in the field, Kenneth Strunk for his help with graphics and Jeffrey Whyatt and Michael Jenkins for their assistance in editing and reviewing a preliminary version of this manuscript.

References

[1]. Benton, D.; Iverson, S.; Johnson, J.; Martin, L. Photogrammetric monitoring of rock mass behavior in deep vein mining. Proceedings of the 33rd International Conference on Ground Control in Mining; Morgantown. WV: West Virginia University; 2014. p. 221-227.

[2]. Kaiser PK, Cai M. Design of rock support system under rock burst conditions. J Rock Mech Geotech Eng. 2012; 4(3):215–27.

[3]. Kirsten H. Comparative efficiency and ultimate strength of mesh and fibre-reinforced shotcrete as determined from full-scale bending tests. JS Afr Inst Min Metall. 1992; 11/12(92):303–23.

[4]. Kirsten H. Equivalence of mesh and fibre reinforced shotcrete at large deflections. Can Geotech J. 1993; 30:418–40.

[5]. Tannant, D.; Kaiser, PK. Evaluation of shotcrete and mesh behaviour under large imposed deformations. International symposium on rock support–Applied solutions for underground structures; Broch E Myrvang Astjern G; 1997. p. 782-92.

[6]. Martin, L.; Clark, C.; Johnson, J.; Stepan, M. Proceedings of Mining & Exploration Technology: Technology Development and Implementation in Rock Mechanics and Ground Control. Denver: 2015. A new high force and displacement shotcrete test; p. 15-090.p. 10

[7]. Birch, J. Laser and photogrammetric methods for rock tunnel characterization. American Rock Mechanics Association; 2008. Using 3DM analyst mine mapping suite for underground mapping.

[8]. Charlie, Li; Chun, L. A new energy-absorbing bolt for rock support in high stress rock masses. Int J Rock Mech Mining Sci. 2010; 47:396–404.

[9]. Anon.. Instruction Manual for Model 4420 Vibrating Wire Crackmeter. Geokon Inc; 2013. p. 1-19.

[10].

Board M. Email correspondence regarding mine conditions. 04–03–2015.

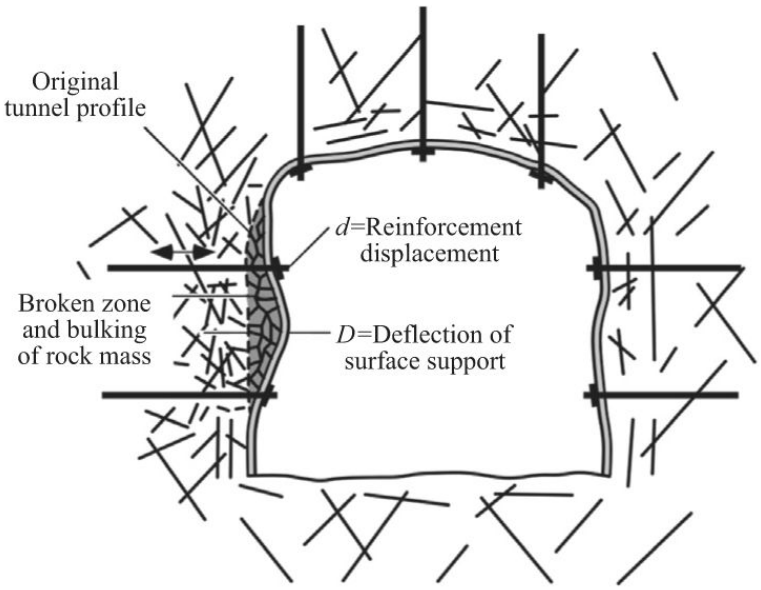

Fig. 1.
Diagram of the reinforced shotcrete system [2].

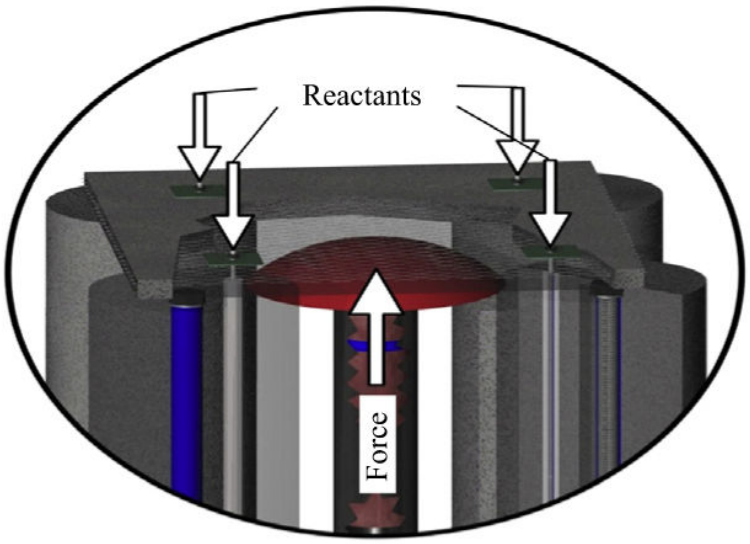

Fig. 2.
Diagram of the force during the high-energy displacement panel test and tester.

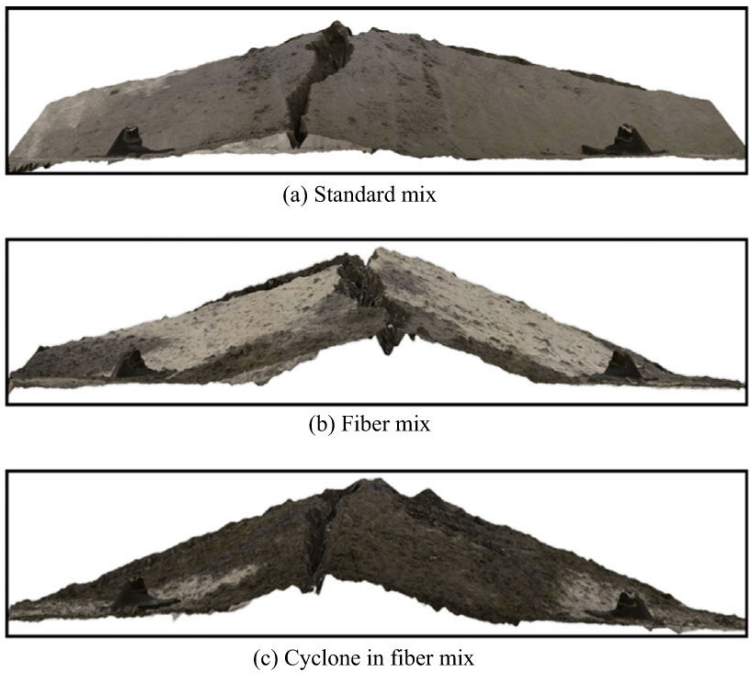

Fig. 3.
Side view of each panel type at 25 cm ram displacement.

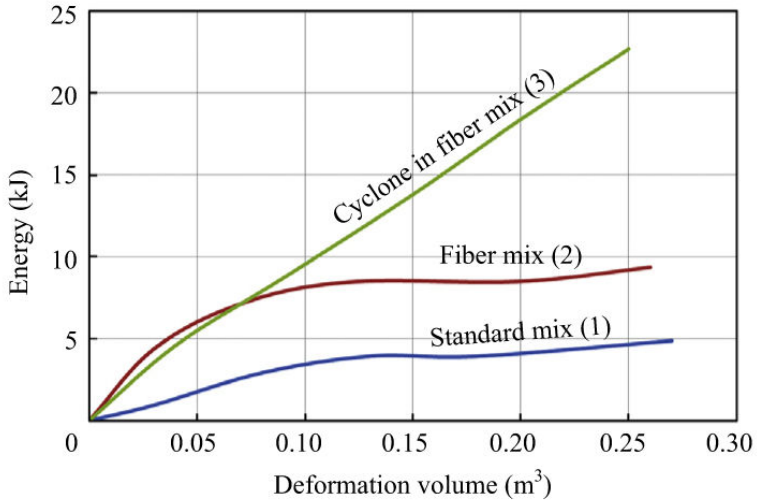

Fig. 4.

Relationship between energy and volume for shotcrete support systems, as determined through photogrammetric measurement.

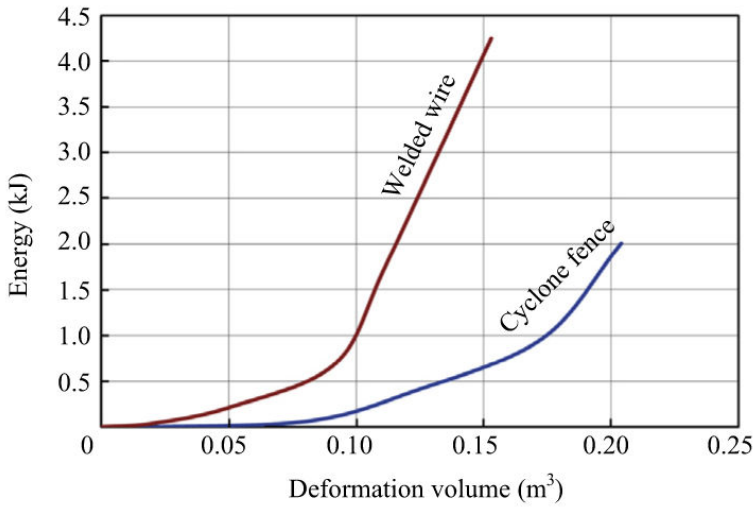

Fig. 5.

Relationship between energy and deformation volume for cyclone fence and welded wire support systems, as determined through photogrammetric measurement.

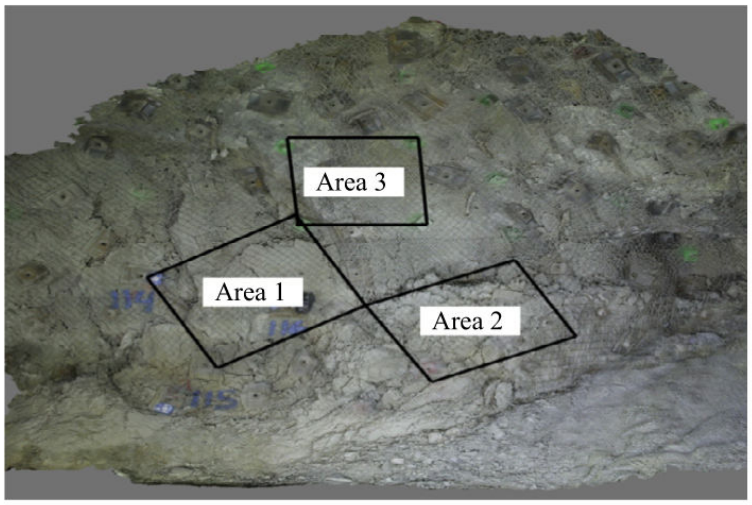

Fig. 6.
Selected rib for volumetric deformation analysis.

(a) Area 1 significant deformation

(b) Area 2 severe deformation

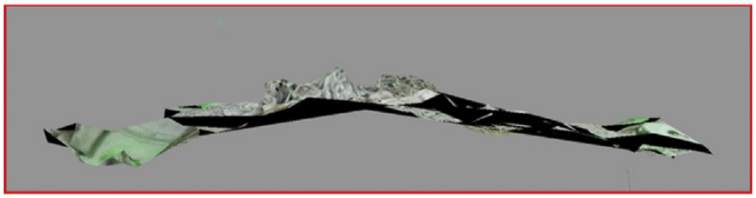

(c) Area 3 minimal deformation

Fig. 7.

Side views of deformation areas selected for field deformation monitoring volume calculations.

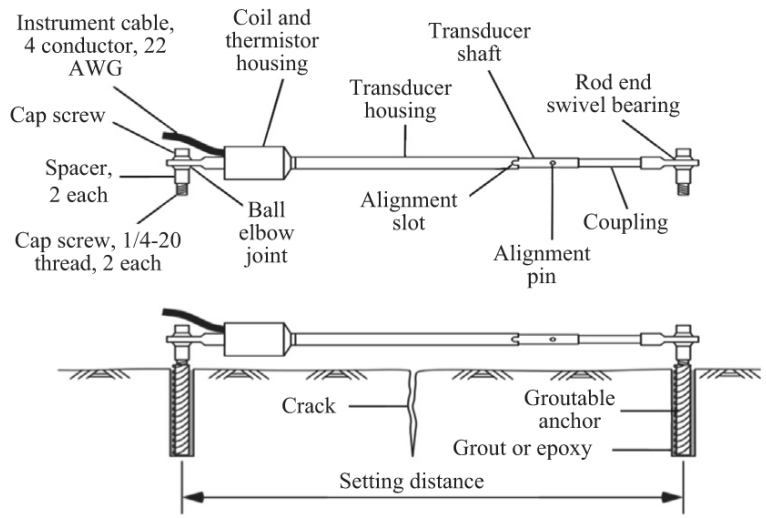

Fig. 8.

Crackmeter schematics showing instrument components and installation [9].

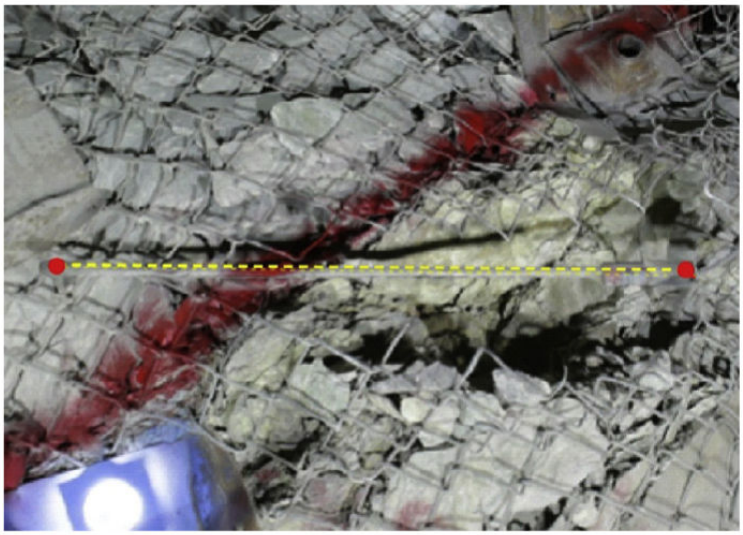

Fig. 9.
Crackmeter installation (yellow dotted-line) across fault (red spray paint).

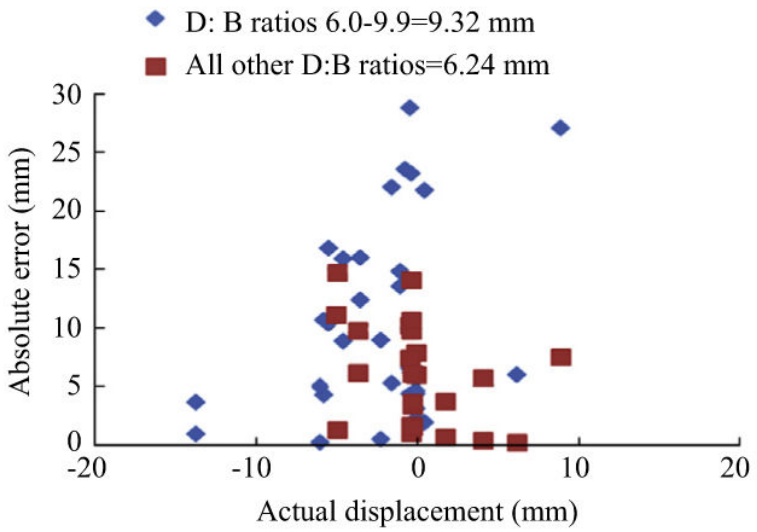

Fig. 10.

Comparison of photogrammetric error and actual crackmeter displacement, coded by D:B ratio, reveals and average error of 8 mm.

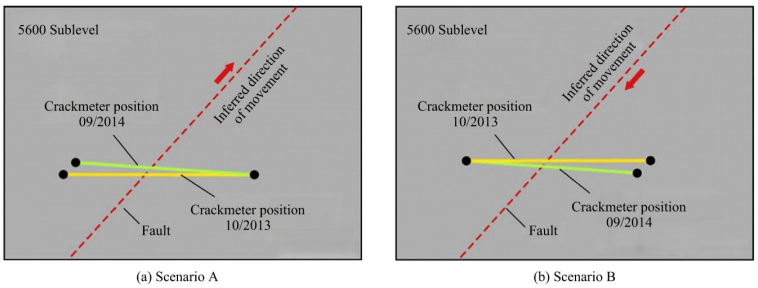

Fig. 11.

Representations of 5600 sublevel crackmeter analysis based on observed shortening of the crackmeter.

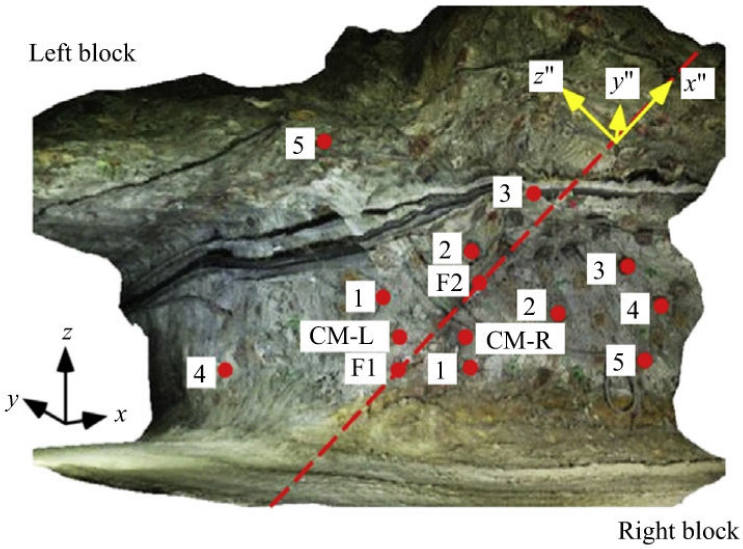

Fig. 12.

Illustration of measuring points (red dots), global axis system (lower-left in black), local axis system (upper-right in yellow) and left and right fault blocks at the 5600 sublevel site.

Table 1

Deformation volumes and energy for each shotcrete panel type at 5 cm intervals (cm).

Item	Standard mix (cm)					Fiber mix (cm)					Cyclone in fiber mix (cm)				
	5	10	15	20	25	5	10	15	20	25	5	10	15	20	25
Min. volume (m^3)	0.029	0.079	0.128	0.177	0.265	0.029	0.069	0.118	0.196	0.255	0.039	0.008	0.147	0.196	0.246
Max. volume (m^3)	0.031	0.081	0.132	0.183	0.275	0.031	0.071	0.122	0.204	0.265	0.041	0.092	0.153	0.204	0.254
Energy (J)	938	2910	3932	3928	4867	4379	7117	8447	8493	9358	4586	8707	13,793	18,386	22,675

Table 2

Deformation volumes and energy for each mesh type at 5 cm intervals.

Item	Cyclone fence (cm)					Welded wire (cm)				
	5	10	15	20	25	5	10	15	20	25
Min. volume (m^3)	0.020	0.079	0.118	0.167	0.196	0.020	0.049	0.088	0.108	0.147
Max. volume (m^3)	0.020	0.081	0.122	0.173	0.204	0.020	0.051	0.092	0.112	0.153
Energy (J)	Negligible	Negligible	384.0	968.0	2011	Negligible	219.0	699.0	1792	4250

Table 3

Deformation volumes, height and estimated energy for each area used for field deformation volume calculation.

Item	Area 1	Area 2	Area 3
Min.volume (m^3)	0.231	0.361	0.013
Max. volume (m^3)	0.239	0.375	0.013
Estimated energy (J)	3000	8900	<100

Table 4

Overview of field photogrammetry equipment.

Camera type	**Nikon D80 digital SLR**	**Canon EOS 5D Mark III**
Len	Sigma 10 to 20 mm zoom	Canon Ultrasonic 20 mm
Effective image pixel	10.2 million	22.3 million
Average number of data points per reconstruction	250,000	550,000

Table 5

Global and local coordinate displacements of points at the 5600 sublevel crackmeter site.

(a)

Item	Left block average (cm)	Right block average (cm)	L–R relative movement (cm)
Local (dip, strike, dilation)	9.8	17.7	−7.9
	−6.7	−21.5	14.8
	0.3	−7.5	7.8

(b)

Item	Point	Left block						Right block					
		1	2	3	4	5	CM-L	1	2	3	4	5	CM-L
Global (easting, northing, elevation)	*X* (cm)	0.3	−2.7	−9.8	2.7	−3.7	−9.1	−9.5	−14.3	−12.8	−10.4	−13.1	−12.1
	Y (cm)	−5.8	−8.8	−6.7	−6.1	3.1	−20.2	−19.2	−25.0	−21.0	−25.6	−29.0	−22.8
	Z (cm)	8.5	7.0	0.6	16.5	2.7	15.2	15.9	11.6	5.8	7.0	10.1	15.7
Local (dip, strike, dilation)	*x*” (cm)	10.1	9.5	1.3	17.5	0.0	20.2	20.2	18.2	11.8	15.5	19.1	21.2
	y” (cm)	−2.4	−6.5	−11.7	−0.3	−1.9	−17.2	−17.1	−24.1	−21.0	−20.9	−24.8	−21.1
	z” (cm)	0.0	−1.9	−1.0	3.1	5.2	−3.7	−20.5	−7.2	−7.9	−11.6	−11.5	−10.2